RESEARCH ARTICLE

International Journal of Climatology | RMetS

Local decadal prediction according to statistical/dynamical approaches

Dario Redolat[1,2] | **Robert Monjo[1,3]** | **Cesar Paradinas[1]** | **Javier Pórtoles[1]** | **Emma Gaitán[1]** | **Carlos Prado-Lopez[1]** | **Jaime Ribalaygua[1]**

[1]Climate Research Foundation (FIC), Madrid, Spain

[2]Department of Earth Physics, Astronomy and Astrophysics II, Complutense University of Madrid, Madrid, Spain

[3]Department of Algebra, Geometry and Topology, Complutense University of Madrid, Madrid, Spain

Correspondence
Dario Redolat, Climate Research Foundation (FIC), Madrid, Spain.
Email: dario@ficlima.org

Funding information
H2020 European Research Council, Grant/Award Number: 700174

Abstract

Dynamical climate models present an initialization problem due to the poor availability of deep oceanic data, which is required for the model assimilation process. In this sense, teleconnection indices, defined from spatial and temporal patterns of climatic variables, are conceived as useful tools to complement them. In this work, the near-term climate predictability of 35 temperature and 36 precipitation time series of three cities (Barcelona, Bristol and Lisbon) was analysed using two approaches: (a) a statistical–dynamical combination of self-predictable teleconnection indices and long-term climate projections on a local scale and (b) dynamical model outputs obtained from drift-corrected decadal experiments. Fourier and wavelet analyses were used to assess the predictability of seven teleconnection indices thanks to a cross-validation process (with differentiated training and validation periods). The standardized absolute error of teleconnection-based prediction was compared with that obtained from a (9) multi-model ensemble based on the Coupled Model Intercomparison Project Phase 5. Results showed that decadal predictions at horizons between 20 and 30 years are adequate for temperature and precipitation if a teleconnection-based approach is used, while temperature is better predicted from a 5-year horizon using drift-corrected dynamical outputs.

KEYWORDS

cross validation, decadal forecast, statistical hindcast, teleconnection indices

1 | INTRODUCTION

Until recently, climate projections have been the only available source of climate information for reduced time-scales (between the year and the decade). However, in the last 10 years, significant progress has been achieved in what is known as 'decadal prediction'. This term encompasses predictions on annual, multi-annual and decadal timescales (Kim *et al.*, 2012). Decadal simulations are usually carried out with dynamical models with consequent initialization problems. Initialized models have a better ability to predict in short scales than noninitialized models, a feature that diminishes over a longer prediction horizon (Kirtman *et al.*, 2013). This is because the predictability decreases over time due to several uncertainty sources: Natural internal variability, the external forcings

of climate systems and uncertainty in the climate system's response sensitivity to these forcings (Meehl *et al.*, 2009; Doblas-Reyes *et al.*, 2013). The uncertainty sources affect the reliability of climate models, particularly in terms of large timescales, limiting the capacity for possible long-term preventive measures against changes in weather patterns.

Alternatively, statistical methods based on teleconnections can also be used for decadal predictions. Generally, oceanic anomalies show alternant and slow-evolving positive/negative phases, which allows for the forecasting of dominant synoptic patterns in the atmosphere for up to several months or decades. The most popular teleconnection is the El Niño–Southern Oscillation (ENSO), which causes anomalies around the world (Trenberth and Stepaniak 2001). Other phenomena based on oceanic anomalies include the Atlantic Multidecadal Oscillation (AMO) and Pacific Decadal Oscillation (PDO), with clear influences on decadal climate variability (Schlesinger, 1994; Zhang *et al.*, 1997; O'Reilly *et al.*, 2016).

On the other hand, some teleconnections are related to latitudinal energy flows from oceanic or atmospheric circulation patterns. For instance, the Sahel precipitation index (SAHEL-Pi) is a good measure of the effects of latitudinal variation in the Intertropical Convergence Zone (ITCZ), while the Gulf Stream north wall index (GSNWi) represents in the same way the latitudinal variation in the gulf stream of the western Atlantic (Joyce *et al.*, 2009; Taylor, 2011; Mitchell, 2016). Unfortunately, the initial conditions of ocean currents are mostly known, especially in the deep ocean. In fact, decadal experiments offer a low skill when simulating quasi-oscillations, including the PDO or SAHEL (Kim *et al.*, 2012; Gaetani and Mohino, 2013).

In contrast with the oceanic nature, atmospheric anomalies present generally a short memory, which is useful for seasonal forecasts but not for decadal predictions. However, despite their low inertia, some atmospheric phenomena can be coupled to sea surface temperature (SST) fluctuations and consequent feedback, representing some modes of decadal variability and linking distant places (Sun *et al.*, 2015; Redolat *et al.*, 2018). This is the case of the Western Mediterranean Oscillation (WeMO), used to analyse the anomalies in the western Mediterranean (Martin-Vide and Lopez-Bustins, 2006). The WeMO is characterized by long periods and frequencies of occurrence despite its high intra-annual variability. This is also found for the Atlantic Jet Stream Latitude (AJSL), a pattern indicator based on the latitude anomalies of speed wind in the longitude of the North Atlantic Ocean, which has a long periodicity (Redolat *et al.*, 2018).

Therefore, by considering both the oceanic and atmospheric origins of teleconnections, they can directly serve as a basis of statistical methods for decadal forecasting.

Previous works explored the possibility of using teleconnections to analyse decadal variability based on teleconnection indices, thus serving as support for non-initialized models (Switanek and Troch, 2011; van Oldenborgh *et al.*, 2012). This work aims to improve the predictability and thereby increase the resilience in the North Atlantic Europe region thanks to a combination of statistical and dynamical approaches. The analysed region corresponds to the covering area of the RESilience to cope with the Climate Change in Urban arEas (RESCCUE) project (Velasco *et al.*, 2018): The metropolitan regions of Bristol, Barcelona and Lisbon. Three pilot cities (with point observations) were selected for the study instead of a regular grid of large regions (which leads to a worse spatial resolution) because climate information on a local scale is demanded to reinforce resilience to climate-related risks in urban areas. These risks add to the intense urban pressure and high population density that characterize such cities, which translate into challenges that can affect basic services (ARUP and Rockefeller Foundation, 2015).

To identify the local details of the urban climate, key methodologies are based on statistical downscaling techniques, including (systematic) drift-error corrections (Doblas-Reyes *et al.*, 2013; Ribalaygua *et al.*, 2013). The new contribution of this paper is the obtaining of local climate simulations on a decadal timescale by combining teleconnection indices and downscaled dynamical outputs. These outputs were selected from the last available versions of Earth System Models (ESMs) from the Coupled Model Intercomparison Project Phase 5 (CMIP5; Taylor *et al.*, 2012).

2 | STUDY AREA AND DATA

2.1 | Study area

This work was carried out in three cities representative of the dominant climates of Western Europe: Bristol, Barcelona and Lisbon (Figure 1). The first has an oceanic climate (*Cfb* according to the Koppen classification) with regularly distributed precipitation throughout the year and typical cool winters and warm summers due to the effect of the Gulf Stream. The last two are characterized by a Mediterranean climate (*Csa* according to the Koppen classification) that is distinguished by warm winters and hot summers and concentrated precipitation in autumn and winter. However, some differences can be found between Lisbon and Barcelona. Lisbon has a precipitation peak in late autumn and winter that is associated with Atlantic cold fronts (typical of Atlantic coasts). Meanwhile, in Barcelona, the rain falls mainly in 'cut-off'
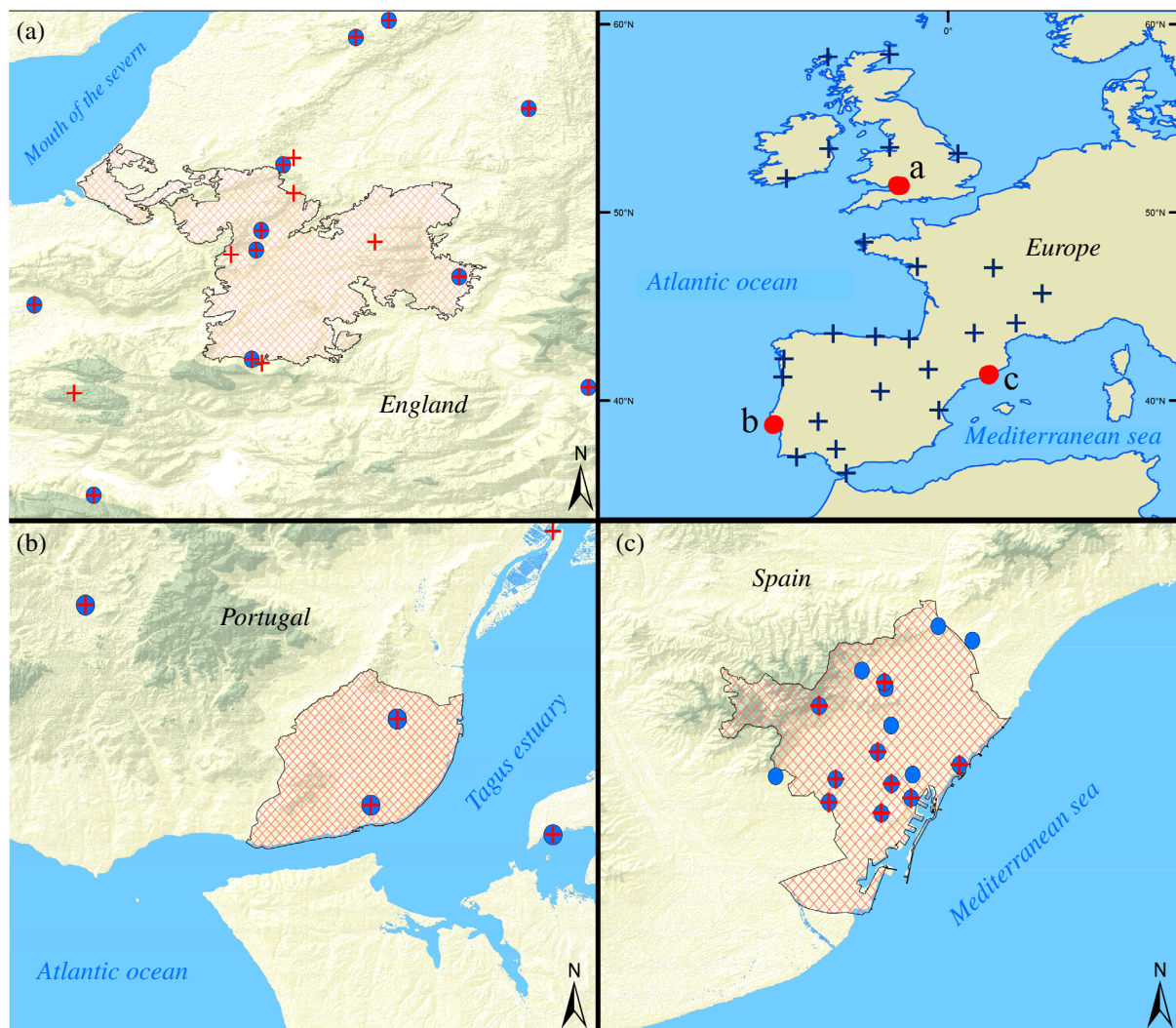
FIGURE 1 Distribution of observed variables along the studied cities. a–c represent Bristol, Lisbon and Barcelona, respectively. The top right represents their location along Western Europe with the main observatories as circles and the comparative observatories as crosses. On the rest of the panels, the temperature observatories are represented by crosses and precipitation by circles. The grid represents the municipality [Colour figure can be viewed at wileyonlinelibrary.com]

patterns, where an isolated upper-level low can produce high and intense levels of rain in a few hours, especially in late summer and the first half of autumn (typical of western Mediterranean coasts).

2.2 | Data

2.2.1 | Observatories

A large database was achieved consisting of temperature and precipitation variables. Several tests were applied to the time series, leaving only stations with good data quality, including general consistency (e.g., possible false zeros, the minimum temperature higher than the maximum temperature, etc.). Particularly, an outlier/

inhomogeneity analysis based on the Kolmogorov–Smirnov (KS) test was performed according to Monjo *et al.* (2013).

Filters were applied to an initial set of 120 time series, and 36 passed the test for temperature and 35 for precipitation. The geographic distribution for the temperature time series contains nine for Barcelona, 22 for Bristol and five for Lisbon. In the case of precipitation, 16 time series were obtained for Barcelona, 14 for Bristol and five for Lisbon. The observations were collected from different sources: Agencia Estatal de Meteorología (AEMET), Instituto Português do Mar e da Atmosfera (IPMA), Global Surface Summary of the Day (NOAA-GSOD) and the Weather Observation Web (MetOffice-WOW). For further spatial analysis of point correlations between teleconnection indices and the climate variables, 25 main

European stations were considered from the Global Surface Summary of the Day (GSOD) and European Climate Assessment & Dataset (ECAD).

2.2.2 | Climate models

In addition to the observed data, surface and atmospheric variables have also been collected from the European ERA-Interim reanalysis and several CMIP5 model outputs, 10 for the climate timescale (2006–2100) and nine for the decadal timescale (2016–2035) (Table 1) and for the corresponding *historical experiment* (1951–2005). Data from climate and decadal scales differ, not only in the horizon considered but also in the total and types of variables used. From the decadal CMIP5 experiments, direct model outputs of precipitation and temperature were used in the drift-correction method (Section 3.2.1). On the other hand, with respect to the CMIP5 climate experiments, atmospheric fields were selected as predictor variables to simulate local climate change (Section 3.2.2), and they were combined with a teleconnection-based method to simulate natural variability at a decadal timescale (Section 3.2.3). Because the projected horizon is up to 20 years, only the Representative Concentration Pathways 4.5 (RCP4.5) is considered. The most basic r1i1p1

run was taken for all climate models except for CanESM2, for which it was the r2i1p1 run.

Decadal experiments (Table 2) are collected considering 10 hindcasts/predictions (approximately every 5 or 10 years) with four different *runs*, which makes 40 available experiments per model in total (except CMCC-CM with just one run and MPI-ESM-LR and MRI-CGCM3 with three runs).

3 | METHODOLOGY

3.1 | General approach

First, a common period was required with a wide enough time range (1979–2015) to serve as a reference for validation processes. As longer time series are generally scarce (with insufficient spatial density), shorter observations were extended using an analogy-based approach applied to the ERA-Interim reanalysis (Section 3.2.1). For this purpose, the original time series length must be at least 5 years of observations (Ribalaygua *et al.*, 2013).

Decadal simulations were developed according to two methods. The first is the drift-correction of annual precipitation and temperature provided by decadal CMIP5 model outputs (Section 3.2.1). The second is a combination of

TABLE 1 Available CMIP5 climate models with outputs on a daily timescale

| Institution | CMIP5 model | | Reference | AGCM resolution (Lon × Lat) | OGCM resolution (Lon × Lat) |
	For climate experiments	For decadal experiments			
CSIRO, BOM	ACCESS1-0	–	Bi *et al.* (2013)	1.87° × 1.25°	*lon(i,j) × lat(i,j)*
BCC	BCC-CSM1-1	BCC-CSM1-1	Xiao-Ge *et al.* (2013)	2.8° × 2.8°	1.0° × 0.33°
CC-CMA	CanESM2	CanCM4	Chylek *et al.* (2011); von Salzen *et al.* (2013)	2.8° × 2.8°	1.41° × 0.93°
CMCC	–	CMCC-CM	Vichi *et al.* (2011) Bellucci *et al.* (2012)	0.75° × 0.75°	*lon(i,j) × lat(i,j)*
CNRM-CERFACS	CNRM-CM5	CNRM-CM5	Voldoire *et al.* (2013)	1.4° × 1.4°	*lon(i,j) × lat(i,j)*
GFDL	GFDL-ESM2M	–	Dunne *et al.* (2012)	2° × 2.5°	1.0° × 0.33°
MOHC	HADGEM2-CC	HADCM3	Collins *et al.* (2001); Collins *et al.* (2011)	1.87° × 1.25°	1.0° × 0.33°; 1.25° × 0.25°
IPSL	–	IPSL-CM5A-LR	Dufresne *et al.* (2013)	3.75° × 1.89°	*lon(i,j) × lat(i,j)*
JAMSTEC, AORI, NIES	MIROC-ESM-CHEM	MIROC5	Watanabe *et al.* (2011)	2.8° × 2.8° 1.4° × 1.4°	1.7° × 0.56°; 0.5° × 0.5°
MPI-M	MPI-ESM-MR	MPI-ESM-LR	Marsland *et al.* (2003)	1.8° × 1.8°	*lon(i,j) × lat(i,j)*
MRI	MRI-CGCM3	MRI-CGCM3	Yukimoto *et al.* (2011)	1.2° × 1.2°	1.0° × 0.5°
NCC	NorESM1-M	–	Bentsen *et al.* (2012), Iversen *et al.* (2012)	2.5° × 1.9°	*lon(i,j) × lat(i,j)*

Note: The table shows the responsible institution, climate/decadal model version, respective references and their spatial resolutions for the AGCM and the OGCM. The case of lon(i,j) × lat(i,j) denotes longitudes and latitudes depending on each grid point (represented as indices i and j).

TABLE 2 Indices and their variables considered: SST is sea surface temperature, SLP represents sea level pressure, R is annual rainfall and WS is wind speed at 300 hPa

Index	Start	End	Used variable	Used region	References
PDOi	1854	2016	SST	Pacific 20°N	Mantua and Hare (2002)
ENSOi	1870	2015	SST	El Niño 3.4 (170°W to 120° W-EQ)	Wolter and Timlin (2011)
AMOi	1870	2015	SST	Atlantic 0°–60°N and 7.5°W–7.5°E	Rayner *et al*. (2003)
GSNWi	1966	2010	SST	Atlantic 55° to 75°W–35°N	Taylor (2011)
WeMOi	1821	2013	SLP	Padua–San Fernando	Martin-Vide and Lopez-Bustins (2006)
SAHEL-Pi	1901	2016	R	Africa 8°–20°N–20°W to 10°E	Becker *et al*. (2013)
AJSLi	1871	2015	WS	Atlantic 4° to 53°W–45°N to North Pole	Redolat *et al*. (2018)

downscaled CMIP5 climate models (Section 3.2.2) and self-predicted teleconnection indices (Section 3.2.3) to simulate natural variability at a decadal timescale.

3.2 | Statistical downscaling methods

### 3.2.1 | Decadal dynamical output correction

The data assimilation carried out for the initialization of decadal experiments causes a *drift* in the bias of the simulated variables until they are stabilized (Kim *et al*., 2012; Doblas-Reyes *et al*., 2013). The drift is produced until the model simulates enough transitory time since the beginning of the run (around a 10-year horizon). As decadal experiments predict for up to 30 years, it is necessary to consider and correct this drift (Figure 2a).

Because the bias drift depends on the yearly temporal horizon, daily data are aggregated into a yearly scale, and to keep the natural signal of the variable, the *time horizon* was redefined as a temporal unit of prediction; the value at the *i*-horizon (H_{kj}) is calculated as the mean of the *i* previous years (Equation (1)).

$$H_{kj} = \frac{1}{k}\sum_{j=1}^{k} h_{kj} \qquad (1)$$

This is important because the climatic signal weakens over the time horizon, and it is not possible to distinguish the annual resolution for many years.

All horizons for each model are rearranged so only the 10 *i*-year horizons are computed together (where *i* = 1,...,10) for each run (Doblas-Reyes *et al*., 2013). These *i*-horizon series are corrected by parametric quantile mapping between simulated and observed ones, distinguishing among each *i*-year horizon (Figure 2b,c). Horizons from 11 to 30 years (2005–2035) were corrected using the values obtained with *i* = 10. The KS test was applied to select the
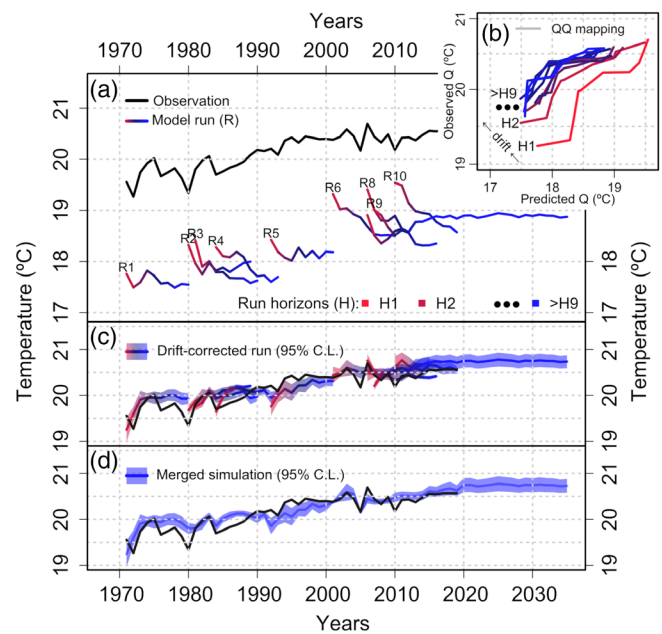
FIGURE 2 Schematic example of the drift-correction method. Box (a) represents a comparison between 10 different runs and observations; box (b) represents the correlation between the quantile–quantile predicted temperature (*X*-axis) and observed temperature (*Y*-axis); box (c) represents the drift correction applied to each run; box (d) represents the final results with the corrections merged to the prediction [Colour figure can be viewed at wileyonlinelibrary.com]

most reliable parametric distribution (Marsaglia *et al*., 2003; Monjo *et al*., 2014). Due to the softness of the aggregated climate signal (H_{kj}), a normal distribution was enough to be considered for correcting temperature and a lognormal distribution for precipitation.

As some models show overlapping experiments with different values, an estimation of the median and dispersion was obtained for the 1986–2035 period using nine CMIP5 models running at decadal scale (Table 1). For the dispersion, a 10–90% range is estimated combining the set of overlapping experiments and the uncertainty

level obtained from the drift correction (Figure 2d). The final aggregated climate signal and the further corrected ensemble are additional statistical treatments respect to the previous works of drift correction.

3.2.2 | Analogy-based approach

This work uses the two-step statistical downscaling method developed by Ribalaygua *et al.* (2013), which is summarized here.

Analogue stratification

The first step, which is common for temperature and precipitation, is based on an analogue stratification (Zorita *et al.*, 1993). That is, *n* analogue days (the most similar ones to the day to be downscaled) are selected to reduce non-linearity. The similarity between 2 days was measured using a weighted Euclidean distance according to three nested synoptic windows and four large-scale fields used as predictors: The (a) speed and (b) direction of geostrophic wind at 1,000 hPa and the (c) speed and (d) direction of geostrophic wind at 500 hPa. For each predictor, the distance was calculated and standardized by replacing it with the closest centile of a reference population of distances for that predictor. The four predictors were finally equally weighted, while the synoptic windows had different weights.

Temperature function

In the second step, a transfer function (linear by stepwise regression) is applied for $n = 150$ analogous days. Choosing the most similar days, considering precipitation and cloudiness, reduces the non-linearity of the links between free atmosphere and surface variables on a local scale. Thanks to temperature being near-normally distributed, linear regressions perform well in estimating the maximum and minimum values; this also obligates taking the near-normal distributed predictors.

    1.1,000/500 hPa thickness above the surface station.

    2.1,000/850 hPa thickness above the surface station.

    3.A sinusoid function of the day of the year.

    4.A weighted average of the station mean of daily temperatures of the 10 previous days.

    Diagnostic equations are calculated (using the predicting and predictor values with a population of *n* analogue days) and applied to estimate daily temperatures for each station and problem day.

Precipitation function

In the second step, a group of *m* problem days was downscaled together (all days of a month were used). For each problem day, a 'preliminary precipitation amount' was obtained, averaging the rain amount on its *n* most analogous days, so the *m* problem days can be sorted from highest to lowest in terms of 'preliminary precipitation amount'. In addition, for assigning the final precipitation amount, all amounts of the $m \times n$ analogous days are sorted and clustered into *m* groups. Every quantity is finally assigned orderly to the *m* days previously sorted by the 'preliminary precipitation amount.'

    Assuming there is little variation in the climatic characteristics of rainfall within a month, the $n \times m$ analogous days of a month can be mixed to obtain a better probability distribution (or Empirical Cumulative Distribution [ECDF]). Therefore, the number of problem days is chosen as $m = 30$. Systematic error or bias was corrected for all climate simulations of temperature and precipitation using parametric quantile mapping (Monjo *et al.*, 2014, 2016).

3.2.3 | Teleconnection-based method

A purely statistical approach was used to simulate natural variability on a decadal timescale, adding to local climate change (Section 3.2.1). In total, seven (four ocean-based and three atmospheric-based) teleconnection indices were chosen for this study (Table 2). Fourier and wavelet analyses were applied to fit and predict the natural variability of these teleconnections in the future. This approach has been employed in previous works to examine the interannual or decadal variability of temperature or precipitation in the past, but not yet for decadal prediction (Benner, 1999; van Oldenborgh *et al.*, 2012).

    The selection of these indices is based on the fact that they have decadal-level oscillations capable of explaining movements at these time scales in the coupled ocean–atmosphere system (López-Parages and Rodríguez-Fonseca, 2012). In this sense, the indices that best explain the annual and decadal variability are usually oceanic due to the greater inertia of the ocean. However, there are also atmospheric indices with decadal variability that have been selected using the methods described above.

Theoretical assumption

From a conceptual viewpoint, two hypotheses are assumed: (1) the climate system is a coupled dynamic system $\{x_j(x_k, t)\}$ with small perturbations $|x_j| < < 1$ over a given timescale t and close to equilibrium ($x_j \sim 0$) and (2) the coupling factor $f_j^k = \partial x_j / \partial x_k$ between the variables x_j and x_k is small and almost constant with respect to the perturbation (Equation (2)).

$$\begin{cases} f_j^k \ll \dfrac{\partial x_j}{\partial t} \Big/ \dfrac{dx_k}{dt} \\[2mm] \dfrac{\partial f_j^k}{\partial x_j} \gg f_j^k \end{cases} \tag{2}$$

Thus, the total variation in each teleconnection index x_i can be considered a quasi-oscillation, that is, a perturbation term plus a coupling term (Equation (3)),

$$dx_j = \frac{\partial x_j}{\partial t}dt + \frac{\partial x_j}{\partial x_k}dx_k = i\ \underbrace{\omega_j x_j dt}_{\text{perturbation}} + \underbrace{f_j^k dx_k}_{\text{coupling term}} \quad (3)$$

where $\omega_j = 2\pi i/T_j$ is the proper oscillation frequency and $f_j^k = \partial x_j/\partial x_k$ is the factor coupling of x_j with respect to x_k.

The sum of all contributions of the variation dx_j leads to a multi-harmonic time series plus a residue that is assumed noise (unpredicted variance of the model).

Harmonic fitting

By neglecting the noise to model the temporal evolution of each teleconnection index (x_j), N simple harmonic functions are obtained from the fitting parameter oscillation frequencies (ω_k), initial phases/times (t_k) and amplitudes (C_k) according to Equation ((4)).
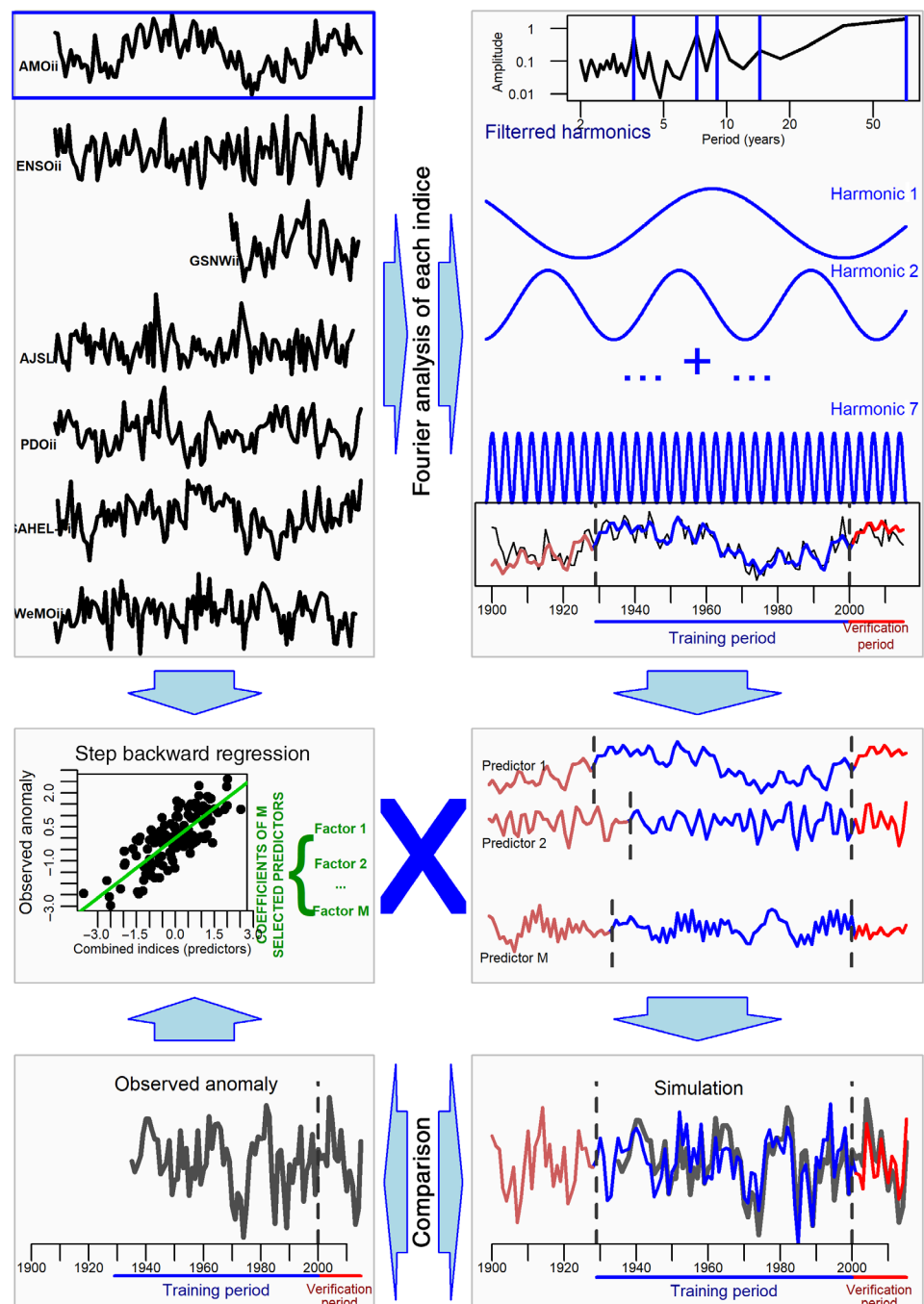
FIGURE 3 Schematic example of the teleconnection-based method. The top left box represents the raw teleconnection indices; the top right box represents the filtered process based on the harmonics; the middle left box shows the backward stepwise regression; the middle right box represents an example of obtained predictors; the bottom left box shows an example of an observed anomaly and the bottom right figure represents a final simulation of the index [Colour figure can be viewed at wileyonlinelibrary.com]

$$x_j \approx \sum_{k=1}^{N} v_j := \mathrm{Re} \sum_{k=1}^{N} C_j \exp(i\omega_k(t-t_k)) \qquad (4)$$

To obtain these simple harmonics, two stages were considered. In the first stage, a periodogram was taken from the Fast Fourier Transform (FFT), and it was filtered using Monjo's spell function (Monjo, 2016; Redolat *et al.*, 2018). Specifically, a factor of two was considered to determine dry/wet spells in the periodogram, and the greatest seven amplitudes were selected (i.e., $N = 7$ was chosen). The temporal stability of significant periods was analysed via a wavelet according to WaveletComp, an R-language package (Rosch and Schmidbauer, 2018).

In the second stage, significant amplitudes were fitted from a backward stepwise regression. Linear regression is enough to fit the initial times t_k thanks to the mathematical properties of trigonometric functions in a complex variable (Equation (5)).

$$x_j \approx \sum_{k=1}^{N} v_k := \mathrm{Re} \sum_{k=1}^{N} C_k$$
$$\exp(i\omega_k(t-t_k)) = \sum_{k=1}^{N} C_k \cos(\omega_k t - \omega_k t_k) =$$
$$\sum_{k=1}^{N} \left[\underbrace{C_k \cos(\omega_k t_k)}_{A_k} \cos(\omega_k t) + \underbrace{C_k \sin(\omega_k t_k)}_{B_k} \sin(\omega_k t) \right]$$
$$= \sum_{k=1}^{N} [A_k \cos(\omega_k t) + B_k \sin(\omega_k t)]$$
$$(5)$$

where the amplitudes A_k, B_k and C_k; the frequency ω_k; and the initial time t_k are constants (fitting parameters). With this, both the amplitude and the initial time can be fitted using linear regression (Figure 3 top panel). To focus on the decadal variability modes, all teleconnection indices were smoothed using a 5-year moving average.

Decadal anomaly simulation
Given a particular training window (see Section 3.2.1), simulations for 5-year averaged temperature and precipitation anomalies were obtained by computing a backward stepwise regression between the observed time series and each teleconnection index (Figure 3 centre-left panel) to finally be applied to the simulated harmonic series (Figure 3 centre-right panel). These simulations were combined with downscaled CMIP5 climate models. That is, external (forcing) and natural contributions were identified in a separate way: Natural variability in the intra-decadal timescale was assumed by the teleconnection-

based simulations (Figure 3 bottom-right panel), while external forcing effects (RCP4.5) were represented by 30-year moving windows averages obtained from downscaled CMIP5 climate models (Section 3.2.1). Note that the scale of 30 years is considered enough to soften the internal variability provided by the dynamical models used.

3.2.4 | Performance and uncertainty analysis

Temporal cross validation
Each detrended and standardized teleconnection index was simulated using the corresponding harmonic model according to the above section. Then, two periods were considered: The training and the validation windows. Both time windows were backward moving to cross validate each harmonic model (hindcast). Several window sizes were tested to find the optimal window size for training the harmonic model of each teleconnection index. Particularly, the set of sizes ranged one-to-one from 20 to $M_j - 10$ years, where $M_j > 50$ years is the total time series length of each index x_j; that is, a minimum of 10 years was reserved to validate the model performance.

On the other hand, the temperature and precipitation variances (predictands) of each station were separately analysed so they could be explained by the best set of teleconnection indices (predictors). For this purpose, a backward stepwise regression was applied between predictors and predictands within each training window. Therefore, temperature and precipitation hindcasts were performed to validate (within the validation windows) their predictability according to the several time horizons and time resolutions of prediction.

The cross validation provided performance statistics, such as standardized absolute error (SAE; Equation ((6))) and standardized square error (SSE; Equation ((7))), which correspond to the explained anomaly (EA = 1 − SAE) and explained variance (EV = 1 − SSE^2), respectively.

$$\mathrm{SAE} = \frac{\sum_{i=1}^{N} |s_i - o_i|}{\sum_{i=1}^{N} |\bar{o}_i - o_i|} \qquad (6)$$

$$\mathrm{SSE} = \sqrt{\frac{\sum_{i=1}^{N} (s_i - o_i)^2}{\sum_{i=1}^{N} (\bar{o}_i - o_i)^2}} \qquad (7)$$

where s_i and o_i are the simulation and observation, respectively, in a year 'i' for a time series of N years.

3.2.5 | Uncertainty cascade

The performances of all used methods were analysed by comparing the observed and the simulated-by-reanalysis time series for the period 1979–2015. The mean absolute or relative errors (MAE and MRE) were estimated for both variables as a main measure of the method's performance.

The SAE is estimated for decadal simulations by comparing their MAEs with that obtained from the climatology-based forecast (i.e., zero anomaly). Moreover, the KS test was applied to analyse the performance model according to the statistical significance (p-value >0.05) of the similarity of the (decadal) simulated probability distributions respective to the observed ones (Marsaglia et al., 2003).

For the CMIP5 models used, the validation consists of evaluating the performance of applying the selected method to each climate model output. In addition, because the observed series present gaps, observations were extended/filled using the corrected ERA-Interim reanalysis (common period 1979–2015).

Regarding the projection uncertainty, a climate simulation on a local scale is given by four main sources: (a) the statistical downscaling method used (verification process), (b) the model/run selection and the method/model performance (validation processes), (c) the RCP scenarios considered and (d) the natural climate variability. The last two uncertainty sources have been treated by using the ensemble strategy. That is, once bias correction is applied to all models, a combination (ensemble) of those models provides an estimation of the uncertainty caused by (past and future) climate variability. An ensemble is performed for each RCP scenario.

4 | RESULTS AND DISCUSSION

4.1 | Performance methods

4.1.1 | Downscaled dynamical model outputs

All climate variables are adequately simulated by statistical downscaling. Daily maximum/minimum temperatures showed a bias and MAE lower than 0.2°C and 2°C, respectively, with accurate sub-daily values (MAE around 1°C in winter and 1.5°C in summer). Precipitation presented a bias lower than 10%. For both variables, all of the time series simulated using Era-Interim passed the KS test (p-value >.05) compared with observed daily distributions.

For downscaled climate models, the analysis of KS p values showed that all outputs are valid for temperature, except using GFDL-ESM2M. Precipitation showed more problems for most of the models, especially when using HADGEM2-CC (passing test for less than 50% of stations). In fact, only two model outputs (ACCESS1-0 and MPI-ESM-MR) passed the KS test for more than 70% of analysed stations.

Regarding the drift-corrected decadal experiments, both the maximum and minimum temperatures are well estimated by almost every model for the three cities, except when using BCC-CSM1 outputs for Lisbon and Bristol (Table 3). Otherwise, for precipitation, the method presented worse results due to its more chaotic nature, with just a few models able to represent the variable historical behaviour properly. In fact, only two drift-corrected models have predictive ability for a 7- to 10-year horizon.

4.1.2 | Teleconnection-based statistical outputs

The predictability of teleconnection indices is strongly linked to the type of variable that characterizes them. On a decadal scale, oceanic indices have a better predictability according to their SAE, particularly when SST is considered. As a result, AMOi obtains the best skill score to predict itself, with the lowest SAE values (from 0.2 to 0.5) for horizons of 2–10 years and training windows of 100–160 years, respectively, which is greater than its periodicity of 64 ± 10 years obtained by a wavelet analysis. A similar output can be found for the GSNWi with low-medium SAE values (from 0.4 to 0.6) for horizons of 2 up to 10 years (a wavelet analysis showed periodicity close to 8 years). The WeMOi is an exception among the atmospheric indices, as it has a highly regular periodicity with large time scales (16–20 years). Thus, its optimal predictability (SAE = 0.5) is found in an intradecadal timescale (until 10 years) with a large training window (>160 years). For the remaining indices, there are modest skill scores, with SAE values above 0.6 in most training windows and horizons; that is, only 40% of each oscillation amplitude is predicted. In fact, a wavelet analysis showed important variability in the periodicity of ENSOi (with noisy oscillations of 4–8 years) and of the atmospheric indices, but statistical significance in quasi-oscillations close to 32 ± 4 years for AJSLi, 60 ± 10 years for WeMOi, 8 ± 1 years for GSNWi and 64 ± 10 years for SAHEL-Pi.

Regarding the correlation between indices and variables, the best indices for comparing with the temperature observed are GSNWi, ENSOi, AJSLi and WeMOi, all with p values below 0.05. For precipitation, GSNWi, WeMOi and AJSLi presented the best correlations, with a

p value below 0.1. Finally, in terms of the predictability of meteorological variables, notable differences between the three cities can be seen, especially when referring to precipitation. In Barcelona, the lowest SAE values are for a horizon between 22 and 30 years; for Bristol, these low values are concentrated between 16 and 29 years and for Lisbon, they are limited to a shorter prediction horizon, from 8 to 9 years. For temperature, a common pattern can be seen: The longer the horizon, the smaller the SAE. The lowest SAE values can be seen from 27 to 30 years in Barcelona and in Lisbon. In Bristol, the prediction period is longer than 23–30 years (Figure 4).

TABLE 3 Summary of the validation for the drift-corrected decadal models according to the SAE criteria for precipitation and temperature (maximum and minimum) [Colour table can be viewed at wileyonlinelibrary.com]

Decadal model	Precipitation			Maximum temperature			Minimum temperature		
	Barcelona	Bristol	Lisbon	Barcelona	Bristol	Lisbon	Barcelona	Bristol	Lisbon
BCC-CSM1-1	10	–	6	8	–	–	8	–	–
CanCM4	–	9	–	10	10	10	10	10	10
CMCC-CM	–	–	–	10	9	7	10	9	4
CNRM-CM5	–	5	–	10	2	6	10	2	10
IPSL-CM5A-LR	2	2	6	10	7	10	10	7	10
MIROC5	–	2	6	10	10	10	10	10	9
MPI-ESM-LR	–	–	–	10	6	10	10	6	10
MRI-CGCM3	–	–	–	10	10	4	10	10	4

Note: The process counts the number of consecutive horizons where the model achieves a SAE < 1 in a metropolitan area (averaging time series of all considered stations). Values within the boxes represent the number of horizons with SAE < 1. On the other hand, symbol '–' means that there is no horizon with SAE < 1.
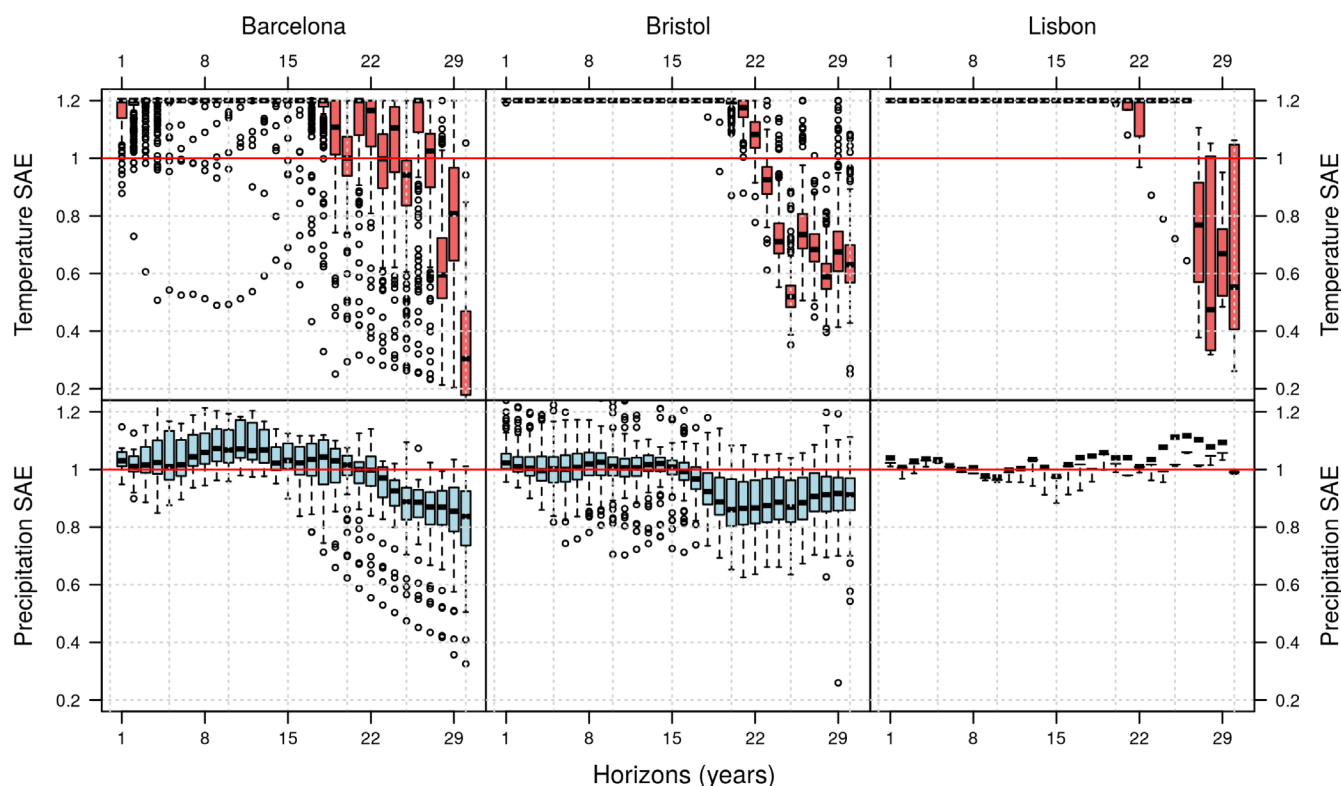

FIGURE 4 Relation between the standardized absolute error (SAE) and horizons (in years) for temperature (first row) and precipitation (second row) for observatories in Barcelona, Bristol and Lisbon (first, second and third columns, respectively) [Colour figure can be viewed at wileyonlinelibrary.com]

Thus, the correlation and statistical significance between teleconnection indices and climate variables has been represented around the RESCCUE cities. In this manner, we observe a common pattern for temperature (Figure 5) in the cities of Bristol and Lisbon, with Barcelona on the opposite side, with antagonistic correlations, that is:

- WeMOi/PDOi with negative correlations in Bristol and Lisbon and positive correlations in Barcelona. A common pattern of inverse correlation can also be observed in southern regions of the Iberian Peninsula, as well as in southern France and Great Britain, being positive in regions of the eastern half of Iberia.

FIGURE 5 Spatial distribution of the Pearson correlation obtained by comparing the observed temperature time series and each index. The bold edges of the circles indicate cases with statistical significance for correlation according to several p values (. 01, .05 and .1) [Colour figure can be viewed at wileyonlinelibrary.com]
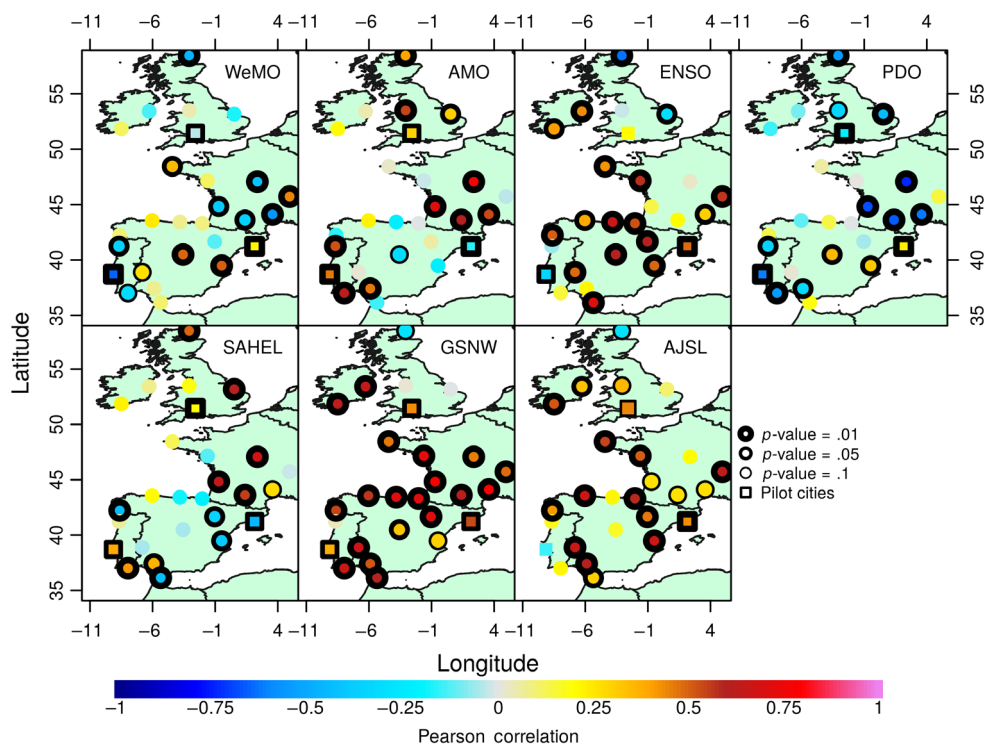
FIGURE 6 Spatial distribution of the Pearson correlation obtained comparing observed precipitation time series and each index. The bold edges of the circles indicate cases with statistical significance for correlation according to several p values (. 01, .05 and .1) [Colour figure can be viewed at wileyonlinelibrary.com]
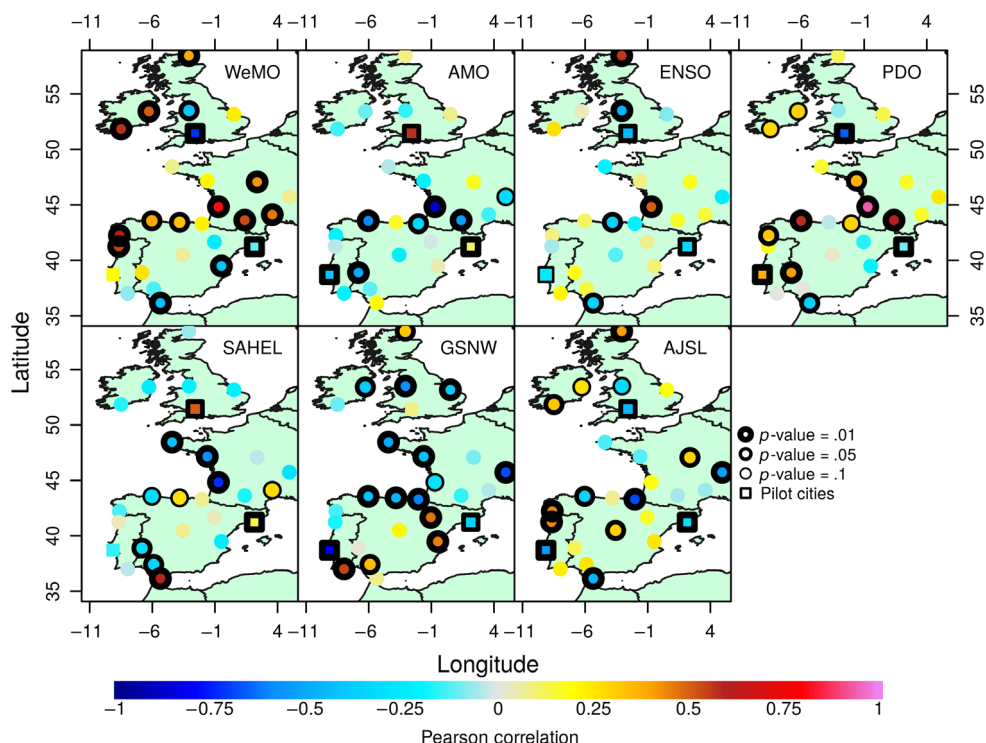
- AMOi/SAHEL-Pi with positive correlations in Bristol and Lisbon and negative correlations in Barcelona. It is also characterized by an almost inverse pattern seen in WeMOi/PDOi with positive patterns in the southwest of the Iberian Peninsula, southern France and Great Britain.
- GSNWi with common positive pattern through three cities. This applies to most Western European observatories.
- Without a characteristic pattern in the ENSOi and AJSLi indices because of the absence of statistical significance. In all other regions, however, positive correlations predominate, except in Great Britain.

Regarding precipitation (Figure 6), a general pattern can be seen in the cities of Barcelona and Bristol, with opposite correlations in Lisbon, that is:

- AMOi with positive correlations in Barcelona and Bristol and negative correlations in Lisbon. SAHEL-Pi with positive correlations in Barcelona and Bristol only and without statistical significance in Lisbon. Although in the rest of the observatories' negative correlations predominate for both indices (especially in the environment of the Bay of Biscay), no predominant geographic pattern is observed due to the lack of significance of numerous observatories.
- PDOi with negative correlations in the three cities. WeMOi with negative correlations in Barcelona and Bristol and without statistical significance in Lisbon. In all other regions, positive values predominate in the Bay of Biscay, including southern France and Ireland for both indices. In the Mediterranean region, as well as in the south of Great Britain, negative correlations predominate.
- ENSOi/AJSLi with common negative correlations in the three cities. In addition, there is a predominance of negative values in the coastal regions of the southwest of Great Britain and the Cantabrian Coast. They are also observed in some Atlantic and Mediterranean observatories, although there is a shortage of significance, especially in the case of ENSO due to the annual scale.
- GSNWi with negative correlations in Barcelona and Lisbon and without statistical significance in Bristol. Negative values predominate in the Bay of Biscay, as well as in parts of Britain and Ireland. In areas of the east and south of the Iberian Peninsula, on the other hand, positive values predominate.

4.2 | Climate decadal scenarios

According to the uncertainty analysis of the predictions, some climate signals could be statistically significant. For Barcelona, the most important change in the future climate of this city is given by the temperature rise. According to the teleconnection-based method, the temperature could increase between 0.2°C and 1°C for 2025–2035 (with respect to the 1979–2015 baseline), while under the drift-correction method, this increase would be limited to between 0°C and 0.9°C. As for precipitation, with a high level of uncertainty, no significant changes are expected in annual rainfall (Figure 7).

In the case of Bristol, the temperature estimates point to a gradual warming, although under the teleconnection method (with great uncertainty), temperature oscillates between 0.2°C and 1.1°C from 2025–2035. Under the drift-correction method, this increase would be limited to between 0.1°C and 1°C. No significant changes are expected in precipitation between now and 2035; however, the teleconnection-based method foresees a possible average increase of up to 5% (Figure 8).

Regarding Lisbon, the temperature could rise between 0°C and 0.3°C according to the teleconnection-based method (Figure 9a). Meanwhile, according to the drift-correction method, the projection is similar, estimating a maximum heating of 0.2°C (Figure 9b). In terms of precipitation, the teleconnection method estimates a possible decrease in rainfall between 2% and 8%, with a median of 4% (Figure 9c); meanwhile, with the drift-corrected method, this decrease oscillates from 0% to 15% with a median of 10% (Figure 9d).

5 | CONCLUSIONS

Near-term climate (decadal) predictions of mean anomalies have been obtained for Barcelona, Lisbon and Bristol using two methods: (a) drift-corrected CMIP5 decadal simulations and (b) a teleconnection-based approach combined with downscaled CMIP5 climate models.

The methods used were verified using surface observations and ERA-Interim reanalysis as a reference for reproducing the past climate. In a similar way, the application of these methods to global climate models was also validated according to several statistical measures. Both processes showed an adequate performance for all simulated climate variables, with negligible systematic errors in the mean climate. Decadal predictions at 20–30 years are adequate for temperature if the teleconnection-based approach is used, while in precipitation, 20–30 years are suitable only in the case of Barcelona and Bristol and 10 years are suitable in the case of Lisbon. The drift-corrected dynamical outputs are better to predict temperature over a horizon of 5 years. This is because temperature anomalies present a lower amplitude/variability than precipitation for decadal timescales. That is, the
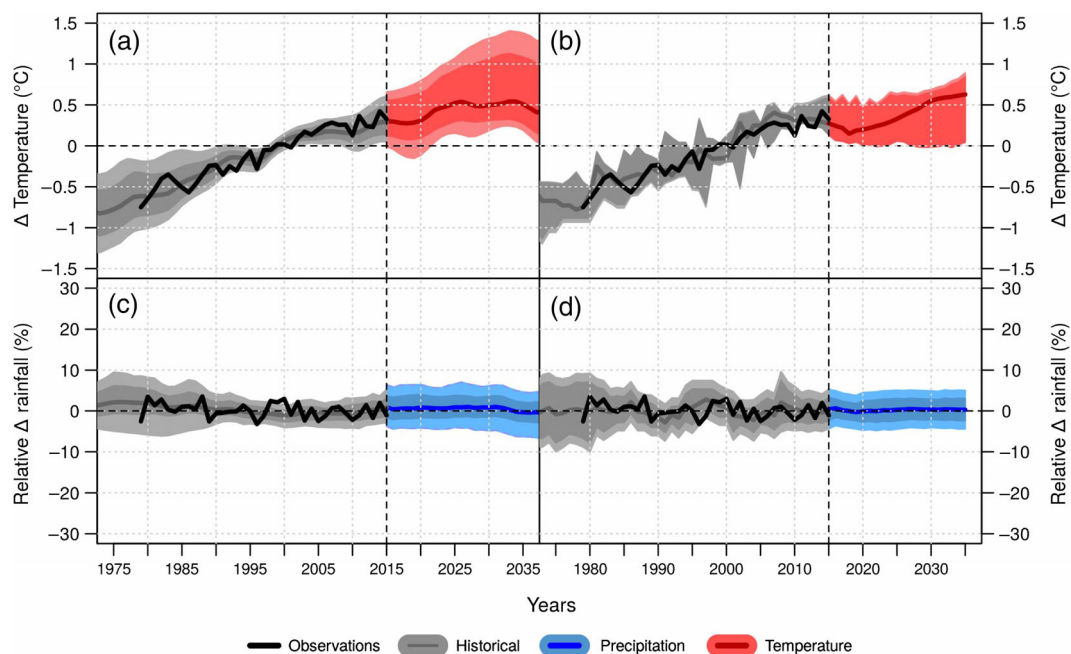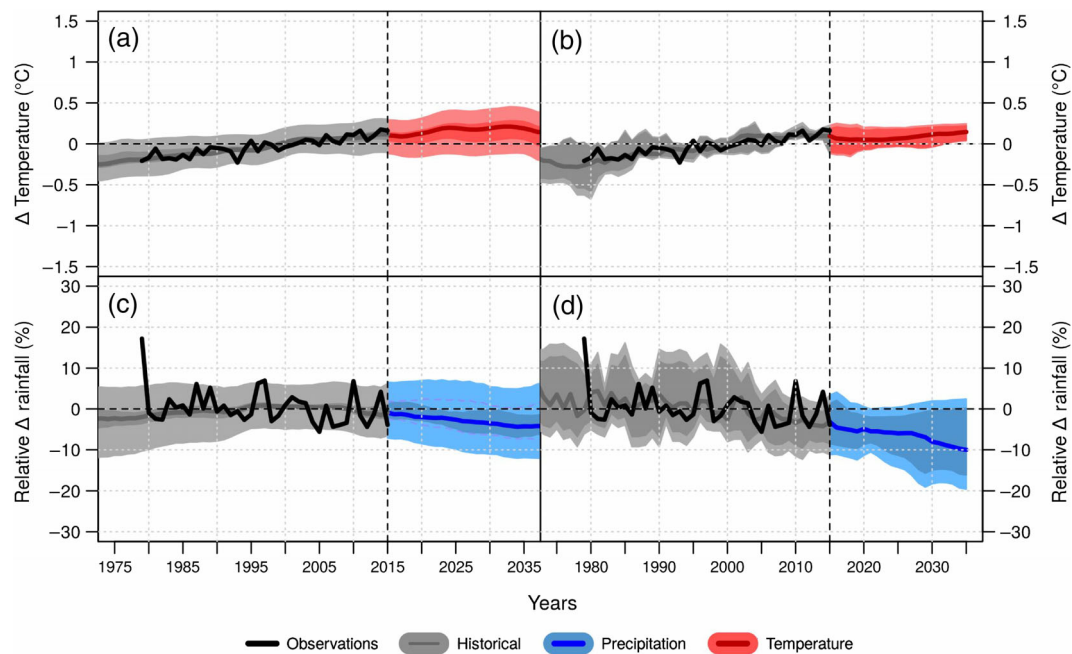
FIGURE 7 Climate projections of changes in maximum temperature (first row) and precipitation (second row) for the teleconnection-based method (a, c) and drift-correction method (b, d) for Barcelona until 2035 (with respect to the 1979–2015 baseline). Data are grouped for the RCP4.5 simulation of every climate model used and for the last 30 years. The ensemble median (solid lines) and the 10th–90th percentile values (shaded areas) are displayed. The vertical dashed line marks the end of the historical data (2015) [Colour figure can be viewed at wileyonlinelibrary.com]
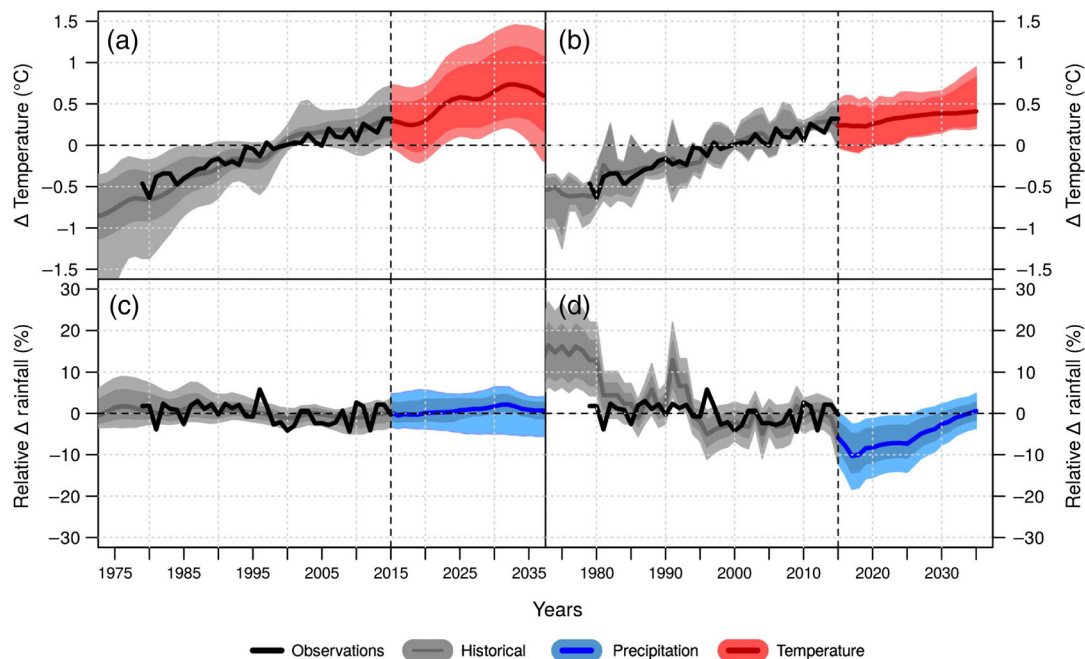
FIGURE 8 Climate projections of changes in maximum temperature (first row) and precipitation (second row) for the teleconnection-based method (a, c) and drift-correction method (b, d) for Bristol until 2035 (with respect to the 1979–2015 baseline). Data re grouped for the RCP4.5 simulation of every climate model used and for the last 30 years. The ensemble median (solid lines) and the 10th–90th percentile values (shaded areas) are displayed. The vertical dashed line marks the end of the historical data (2015) [Colour figure can be viewed at wileyonlinelibrary.com]

FIGURE 9 Climate projections of changes in maximum temperature (first row) and precipitation (second row) for the teleconnection-based method (a, c) and drift-correction method (b, d) for Lisbon until 2035 (with respect to the 1979–2015 baseline). Data are grouped for the RCP4.5 simulation of every climate model used and for the last 30 years. The ensemble median (solid lines) and the 10th–90th percentile values (shaded areas) are displayed. The vertical dashed line marks the end of the historical data (2015) [Colour figure can be viewed at wileyonlinelibrary.com]

detrended temperature approaches zero compared to the detrended annual rainfall, which presents strong multi-decadal oscillations and, therefore, the correlation is more frequently (statistically) significant for signals very different from zero.

In addition, a differentiated spatial pattern of the impacts of the indices on the variables can be found in Western Europe. For instance, the correlation with temperature showed a predominant tripole among the Southwestern Iberian Peninsula, Eastern Iberian Peninsula and Southern France for WeMOi, AMOi, PDOi and SAHEL-Pi.

Regarding the predictability of the teleconnection indices, those based on SST presented the maximum prediction horizon with a minimum SAE (down to 20% of the error in the predicted oscillation amplitude). However, atmospheric indices also presented significant results in the predictability of a decadal timescale. This is because they are partially forced by oceanic variables, with a slow evolution of oscillation amplitudes (great memory/inertia in the positive–negative phase transition).

Altogether, both teleconnection-based outputs and the drift corrections showed that temperature could rise by a range of 0°C to 1°C in Barcelona and Bristol and from 0° to 0.5°C in Lisbon for the 2016–2035 period. Therefore, both methods show an increase in temperature with a high uncertainty level due to natural variability.

In the case of precipitation, the teleconnection method shows decreases for the city of Lisbon (4%) and no significant changes expected for Barcelona and Bristol. All of these results are characterized by a high level of uncertainty. However, the combination of downscaled dynamical models with (purely statistical) teleconnection-based methods provides a way to measure and manage the uncertainty thanks to the consensus criteria, that is, when two different methods (with respective ensemble prediction) lead to the same forecast, it reduces uncertainties related to systematic errors of the median prediction (from the choice of method).

ORCID
Dario Redolat https://orcid.org/0000-0001-9621-8730

REFERENCES
ARUP and Rockefeller Foundation. (2015) *City Resilience and the City Resilience Framework: 100 Resilient Cities*. New York: ARUP.

Becker, A., Finger, P., Meyer-Christoffer, A., Rudolf, B., Schamm, K., Schneider, U. and Ziese, M. (2013) A description of the global land-surface precipitation data products of the Global Precipitation Climatology Centre with sample applications including centennial (trend) analysis from 1901–present. *Earth System Science Data*, 5, 71–99. https://doi.org/10.5194/essd-5-71-2013.

Benner, T.C. (1999) Central England temperatures: long-term variability and teleconnections. *International Journal of Climatology*, 19, 391–403. https://doi.org/10.1002/(SICI)1097-0088(19990330)19:4<391::AID-JOC365>3.0.CO;2-Z.

Bentsen, M., Bethke, I., Debernard, J.B., Iversen, T., Kirkevåg, A., Seland, Ø., Drange, H., Roelandt, C., Seierstad, I.A., Hoose, C. and Kristjánsson, J.E. (2012) The Norwegian Earth System Model, NorESM1-M – Part 1: Description and basic evaluation. *Geoscientific Model Development Discussion*, 5, 2843–2931. https://doi.org/10.5194/gmdd-5-2843-2012.

Bellucci, A., Gualdi, S., Masina, S., Storto, A., Scoccimarro, E., Cagnazzo, C., ... Navarra, A. (2012). Decadal climate predictions with a coupled OAGCM initialized with oceanic reanalyses. *Climate Dynamics*, 40(5-6), 1483–1497. https://doi.org/10.1007/s00382-012-1468-z.

Bi, D., Dix, M., Marsland, S., O'Farrell, S., Rashid, H., Uotila, P., Hirst, A., Kowalczyk, E., Golebiewski, M., Sullivan, A., Yan, H., Hannah, N., Franklin, C., Sun, Z., Vohralik, P., Watterson, I., Zhou, X., Fiedler, R., Collier, M., Ma, Y., Noonan, J., Stevens, L., Uhe, P., Zhu, H., Griffies, S., Hill, R., Harris, C. and Puri, K. (2013) The ACCESS coupled model: description, control climate and evaluation. *Australian Meteorological and Oceanographic Journal*, 63, 41–64.

Chylek, P., Li, J., Dubey, M.K., Wang, M. and Lesins, G. (2011) Observed and model simulated 20th century Arctic temperature variability: Canadian Earth System Model CanESM2. *Atmospheric Chemistry and Physics Discussions*, 11, 22893–22907. https://doi.org/10.5194/acpd-11-22893-2011.

Collins, M., Tett, S.F.B. and Cooper, C. (2001) The internal climate variability of HadCM3, a version of the Hadley Centre coupled model without flux adjustments. *Climate Dynamics*, 17, 61–81. https://doi.org/10.1007/s003820000094.

Collins, W.J., Bellouin, N., Doutriaux-Boucher, M., Gedney, N., Halloran, P., Hinton, T., Hughes, J., Jones, C.D., Joshi, M., Liddicoat, S., Martin, G., O'Connor, F., Rae, J., Senior, C., Sitch, S., Totterdell, I., Wiltshire, A. and Woodward, S. (2011) Development and evaluation of an Earth-System model—HadGEM2. *Geoscientific Model Development*, 4, 1051–1075. https://doi.org/10.5194/gmd-4-1051-2011.

Doblas-Reyes, F.J., Andreu-Burillo, I., Chikamoto, Y., García-Serrano, J., Guemas, V., Kimoto, M., Mochizuki, T., Rodrigues, L.R.L. and van Oldenborgh, G.J. (2013) Initialized near-term regional climate change prediction. *Nature Communications*, 4, 1715. https://doi.org/10.1038/ncomms2704.

Dufresne, J., Foujols, M., Denvil, S., Caubel, A., Marti, O., Aumont, O., Balkanski, Y., Bekki, S., Bellenger, H., Benshila, R., Bony, S., Bopp, L., Braconnot, P., Brockmann, P., Cadule, P., Cheruy, F., Codron, F., Cozic, A., Cugnet, D., de Noblet, N., Duvel, J.-P., Ethé, C., Fairhead, L., Fichefet, T., Flavoni, S., Friedlingstein, P., Grandpeix, J.-Y., Guez, L., Guilyardi, E., Hauglustaine, D., Hourdin, F., Idelkadi, A., Ghattas, J., Joussaume, S., Kageyama, M., Krinner, G., Labetoulle, S., Lahellec, A., Lefebvre, M.-P., Lefevre, F., Levy, C., Li, Z.X., Lloyd, J., Lott, F., Madec, G., Mancip, M., Marchand, M., Masson, S., Meurdesoif, Y., Mignot, J., Musat, I., Parouty, S., Polcher, J., Rio, C., Schulz, M., Swingedouw, D., Szopa, S., Talandier, C., Terray, P., Viovy, N. and Vuichard, N. (2013) Climate change projections using the IPSL-CM5 Earth System Model: from CMIP3 to CMIP5. *Climatic Dynamics*, 40, 2123. https://doi.org/10.1007/s00382-012-1636-1.

Dunne, J.P., John, J.G., Adcroft, A.J., Griffies, S.M., Hallberg, R.W., Shevliakova, E., Stouffer, R.J., Cooke, W., Dunne, K.A., Harrison, M.J., Krasting, J.P., Malyshev, S.L., PCD, M., Phillipps, P.J., Sentman, L.T., Samuels, B.L., Spelman, M.J., Winton, M., Wittenberg, A.T. and Zadeh, N. (2012) GFDL's ESM2 Global Coupled Climate–Carbon Earth System Models. Part I: Physical Formulation and Baseline Simulation Characteristics. *Journal of Climate*, 25, 6646–6665. https://doi.org/10.1175/JCLI-D-11-00560.1.

Gaetani, M. and Mohino, E. (2013) Decadal Prediction of the Sahelian Precipitation in CMIP5 Simulations. *Journal of Climate*, 26, 7708–2219.

Iversen, T., Bentsen, M., Bethke, I., Debernard, J.B., Kirkevåg, A., Seland, Ø., Drange, H., Kristjánsson, J.E., Medhaug, I., Sand, M. and Seierstad, I.A. (2012) The Norwegian Earth System Model, NorESM1-M – Part 2: Climate response and scenario projections. *Geoscientific Model Development Discussion*, 5, 2933–2998. https://doi.org/10.5194/gmdd-5-2933-2012.

Joyce, T.M., Kwon, Y. and Yu, L. (2009) On the relationship between synoptic wintertime atmospheric variability and path shifts in the Gulf Stream and the Kuroshio extension. *Journal of Climate*, 22, 3177–3192. https://doi.org/10.1175/2008JCLI2690.1.

Kim, H.M., Webster, P.J. and Curry, J.A. (2012) Evaluation of short-term climate change prediction in multi-model CMIP5 decadal hindcasts. *Geophysical Research Letters*, 39, L10701. https://doi.org/10.1029/2012GL051644.

Kirtman, S.B., Power, S.B., Adedoyin, J.A., Boer, G.J., Bojariu, R., Camilloni, I., Doblas-Reyes, F.J., Fiore, A.M., Kimoto, M. and Meehl, G.A. (2013) *Near-term Climate Change: Projections and Predictability*. Geneva: IPCC.

López-Parages, J. and Rodríguez-Fonseca, M.B. (2012) Multidecadal modulation of El Niño influence on the Euro-Mediterranean rainfall. *Geophysical Research Letters*, 39, L02704. https://doi.org/10.1029/2011GL050049.

Mantua, N. and Hare, S. (2002) The Pacific Decadal Oscillation (PDO). *Journal of Oceanography*, 58, 35–44.

Marsaglia, G., Tsang, W.W. and Wang, J. (2003) Evaluating Kolmogorov's distribution. *Journal of Statistical Software*, 8, 18.

Marsland, S.J., Haak, H., Jungclaus, J.H., Latif, M. and Roeske, F. (2003) The Max-Planck-Institute global ocean/sea ice model with orthogonal curvilinear coordinates. *Ocean Modelling*, 5, 91–127. https://doi.org/10.1016/S1463-5003(02)00015-X.

Martin-Vide, J. and Lopez-Bustins, J. (2006) The western Mediteranean oscillation and rainfall in the Iberian Peninsula. *International Journal of Climatology*, 26, 1455–1475.

Meehl, G.A., Goddard, L., Murphy, J., Stouffer, R.J., Boer, G., Danabasoglu, G., Dixon, K., Giorgetta, M.A., Greene, A.M., Hawkins, E.D., Hegerl, G., Karoly, D., Keenlyside, N.,

Kimoto, M., Kirtman, B., Navarra, A., Pulwarty, R., Smith, D., Stammer, D. and Stockdale, T. (2009) Decadal prediction: Can it be skillful? *Bulletin of the American Meteorological Society*, 90, 1467–1486. https://doi.org/10.1175/2009BAMS2778.1.

Mitchell, T. (2016) *Sahel precipitation index, Joint Institute for the Study of the Atmosphere and Ocean*. Seattle, WA: University of Washington. https://doi.org/10.6069/H5MW2F2Q.

Monjo, R. (2016) Measure of rainfall time structure using the dimensionless n-index. *Climate Research*, 67, 71–86. https://doi.org/10.3354/cr01359.

Monjo R, Pórtoles J, Ribalaygua J (2013) Detection of inhomogeneities in daily data: a test based in the Kolmogorov-Smirnov goodness-of-fit test. In 9th Data Management Workshop of EUMETNET, El Escorial, 6–8 November 2013, Madrid, Spain.

Monjo, R., Caselles, V. and Chust, G. (2014) Probabilistic correction of RCM precipitation in the Basque Country (Northern Spain). *Theoretical and Applied Climatology*, 117, 317–329. https://doi.org/10.1007/s00704-013-1008-8.

Monjo, R., Gaitán, E., Pórtoles, J., Ribalaygua, J. and Torres, L. (2016) Changes in extreme precipitation over Spain using statistical downscaling of CMIP5 projections. *International Journal of Climatology*, 36, 757–769. https://doi.org/10.1002/joc.4380.

O'Reilly, C.H., Minobe, S., Kuwano-Yoshida, A., & Woollings, T. (2016). The Gulf Stream influence on wintertime North Atlantic jet variability. *Quarterly Journal of the Royal Meteorological Society*, 143(702), 173–183. https://doi.org/10.1002/qj.2907.

Rayner, N.A., Parker, D.E., Horton, E.B., Folland, C.K., Alexander, L.V., Rowell, D.P., Kent, E.C. and Kaplan, A. (2003) Global analyses of sea surface temperature, sea ice, and night marine air temperature since the late nineteenth century. *Journal of Geophysical Research*, 108, 4407. https://doi.org/10.1029/2002JD002670.

Redolat, D., Monjo, R., Lopez-Bustins, J.A. and Martin-Vide, J. (2018) Upper-Level Mediterranean Oscillation index and seasonal variability of rainfall and temperature. *Theoretical and Applied Climatology*, 135, 1059–1077. https://doi.org/10.1007/s00704-018-2424-6.

Ribalaygua, J., Torres, L., Pórtoles, J., Monjo, R., Gaitán, E. and Pino, M.R. (2013) Description and validation of a two-step analogue/regression downscaling method. *Theoretical and Applied Climatology*, 114, 253–269. https://doi.org/10.1007/s00704-013-0836-x.

Rosch A, Schmidbauer H (2018) WaveletComp 1.1: A guided tour through the R package. Available at: http://www.hs-stat.com/projects/WaveletComp/WaveletComp_guided_tour.pdf [].

Schlesinger, M.E., & Ramankutty, N. (1994). An oscillation in the global climate system of period 65–70 years. *Nature*, 367(6465), 723–726. https://doi.org/10.1038/367723a0.

Sun, C., Li, J.P., Feng, J. and Xie, F. (2015) A decadal-scale teleconnection between the North Atlantic oscillation and subtropical eastern Australian rainfall. *Journal of Climate*, 28, 1074–1092. https://doi.org/10.1175/JCLI-D-14-00372.1.

Switanek, M.B. and Troch, P.A. (2011) Decadal prediction of Colorado River streamflow anomalies using ocean-atmosphere teleconnections. *Geophysics Research Letters.*, 38, L23404. https://doi.org/10.1029/2011GL049644.

Taylor, A.H. (2011) *The Dance of Air and Sea: How Oceans, Weather and Life Link Together*. Oxford: Oxford University Press, p. 288.

Taylor, K.E., Stouffer, R.J. and Meehl, G.A. (2012) An overview of CMIP5 and the experiment design. *Bulletin of the American Meteorological Society*, 93, 485–498. https://doi.org/10.1175/BAMS-D-11-00094.1.

Trenberth, K.E., & Stepaniak, D.P. (2001). Indices of El Niño Evolution. *Journal of Climate*, 14(8), 1697–1701. https://doi.org/10.1175/1520-0442(2001)0142.0.co;2.

van Oldenborgh, G.J., Doblas-Reyes, F.J., Wouters, B. and Hazeleger, W. (2012) Decadal prediction skill in a multi-model ensemble. *Climate Dynamics*, 38, 1263. https://doi.org/10.1007/s00382-.

Velasco, M., Russo, B., Martínez, M., Malgrat, P., Monjo, R., Djordjevic, S., Fontanals, I., Vela, S., Cardoso, M.A. and Buskute, A. (2018) Resilience to cope with climate change in urban areas-A multisectorial approach focusing on water-The RESCCUE project. *Water*, 10, 1356–1366. https://doi.org/10.3390/w10101356.

Vichi, M., Manzini, E., Fogli, P.G., Alessandri, A., Patara, L., Scoccimarro, E., ... Navarra, A. (2011). Global and regional ocean carbon uptake and climate change: sensitivity to a substantial mitigation scenario. *Climate Dynamics*, 37(9–10), 1929–1947. https://doi.org/10.1007/s00382-011-1079-0.

Voldoire, A., Sanchez-Gomez, E., Salas y Mélia, D., Decharme, B., Cassou, C., Sénési, S., Valcke, S., Beau, I., Alias, A., Chevallier, M., Déqué, M., Deshayes, J., Douville, H., Fernandez, E., Madec, G., Maisonnave, E., Moine, M.-P., Planton, S., Saint-Martin, D., Szopa, S., Tyteca, S., Alkama, R., Belamari, S., Braun, A., Coquart, L. and Chauvin, F. (2013) The CNRM-CM5.1 global climate model: description and basic evaluation. *Climate Dynamics*, 40, 2091–2121. https://doi.org/10.1007/s00382-011-1259-y.

von Salzen, K., Scinocca, J.F., McFarlane, N.A., Li, J., Cole, J.N.S., Plummer, D., Verseghy, D., Reader, M.C., Ma, X., Lazare, M. and Solheim, L. (2013) The Canadian Fourth Generation Atmospheric Global Climate Model (CanAM4) Part I: Representation of Physical Processes. *Atmosphere-Ocean*, 51, 104–125. https://doi.org/10.1080/07055900.2012.755610.

Watanabe, S., Hajima, T., Sudo, K., Nagashima, T., Takemura, T., Okajima, H., Nozawa, T., Kawase, H., Abe, M., Yokohata, T., Ise, T., Sato, H., Kato, E., Takata, K., Emori, S. and Kawamiya, M. (2011) MIROC-ESM 2010: model description and basic results of CMIP5-20c3m experiments. *Geoscientific Model Development*, 4, 845–872. https://doi.org/10.5194/gmd-4-845-2011.

Wolter, K. and Timlin, M.S. (2011) El Niño/Southern Oscillation behaviour since 1871 as diagnosed in an extended multivariate ENSO index (MEI.ext). *International Journal of Climatology*, 31, 1074–1087. https://doi.org/10.1002/joc.2336.

Xiao-Ge, X., Tong-Wen, W. and Jie, Z. (2013) Introduction of CMIP5 Experiments Carried out with the Climate System Models of Beijing Climate Center. *Advances in Climate Change Research*, 4, 41–49. https://doi.org/10.3724/SP.J.1248.2013.041.

Yukimoto S, Yoshimura H, Hosaka M, Sakami T, Tsujino H, Hirabara M, Tanaka TY, Deushi M, Obata A, Nakano H, Adachi Y, Shindo E, Yabu S, Ose T and Kitoh A (2011) Meteorological Research Institute-Earth System Model Version 1 (MRI-ESM1) - Model Description. Technical Report of MRI, No. 64, 83 pp.

Zhang, Y., Wallace, J.M., & Battisti, D.S. (1997). ENSO-like Interdecadal Variability: 1900–93. *Journal of Climate*, 10 (5), 1004–1020. https://doi.org/10.1175/1520-0442(1997)01 02.0.co;2.

Zorita, E., Hughes, J., Lettenmaier, D. and von Storch, H. (1993) Stochastic downscaling of regional circulation patterns for climate model diagnosis and estimation of local precipitation. *Journal of Climate*, 8, 1023–1042.